Self-sustaining turbulence in a restricted nonlinear model of plane Couette flow

Vaughan L. Thomas,[1] Binh K. Lieu,[2] Mihailo R. Jovanović,[2] Brian F. Farrell,[3] Petros J. Ioannou,[4] and Dennice F. Gayme[1]

[1]*Department of Mechanical Engineering, Johns Hopkins University, Baltimore, Maryland, 21218, USA*
[2]*Department of Electrical and Computer Engineering, University of Minnesota, Minneapolis, Minnesota, 55455, USA*
[3]*School of Engineering and Applied Science, Harvard University, Cambridge, Massachusetts, 02138, USA*
[4]*Department of Physics, National and Kapodistrian University of Athens, Panepistimiopolis, Zografos, Athens, 15784, Greece*

This paper demonstrates the maintenance of self-sustaining turbulence in a restricted nonlinear (RNL) model of plane Couette flow. The RNL system is derived directly from the Navier-Stokes equations and permits higher resolution studies of the dynamical system associated with the stochastic structural stability theory (S3T) model, which is a second order approximation of the statistical state dynamics of the flow. The RNL model shares the dynamical restrictions of the S3T model but can be easily implemented by reducing a DNS code so that it retains only the RNL dynamics. Comparisons of turbulence arising from DNS and RNL simulations demonstrate that the RNL system supports self-sustaining turbulence with a mean flow as well as structural and dynamical features that are consistent with DNS. These results demonstrate that the simplified RNL system captures fundamental aspects of fully developed turbulence in wall-bounded shear flows and motivate use of the RNL/S3T framework for further study of wall-turbulence. © *2014 AIP Publishing LLC*. [http://dx.doi.org/10.1063/1.4898159]

I. INTRODUCTION

The Navier-Stokes (NS) equations provide a comprehensive model for the dynamics of turbulence. Unfortunately, these equations are analytically intractable. They have, however, been extensively studied computationally since the pioneering work of Kim, Moin, and Moser[1] and a number of highly resolved numerical simulations exist, see, e.g., Refs. 2–5. Ever increasing computing power promises to make possible simulation of an even wider range of turbulent flows. However, a complete understanding of the physical mechanisms underlying turbulence in the NS equations, even in simple parallel flow configurations, remains elusive. Thus, considerable effort has been devoted to the search for more tractable models for studying the dynamics of turbulence.

The Linearized Navier-Stokes (LNS) equations are a particularly appealing simplified model because they can be analyzed using well developed tools from linear systems theory.[6,7] These equations have been used extensively to characterize energy growth and disturbance amplification in wall-bounded shear flows, in particular the large disturbance amplification that arises from the non-normal linear operators governing these flows.[8–15] The LNS equations capture the energy production mechanism of the full nonlinear system[16] and linear non-normal growth mechanisms have been shown to be necessary for sub-critical transition to turbulence.[17] Related studies of the LNS equations have also provided insight into the mechanism maintaining turbulence. In particular, investigations involving the Orr-Sommerfeld-Squire equations have illustrated that linear coupling between these operators is required to generate the wall layer streaks that are a necessary component of the process maintaining turbulence in wall-bounded shear flows.[18,19] In this context, the term

"streak" describes a "well-defined elongated region of spanwise alternating bands of low and high speed fluid."[20] The LNS equations have also been used to predict second-order statistics[21] and the spectra of turbulent channel flows.[18,22–26] The above results and a host of others illustrate the power of the LNS equations as a model for studying physical mechanisms in wall-turbulence. While the LNS equations provide insight into a number of aspects of the mechanisms underlying turbulence, there are two fundamental aspects of turbulence that the LNS system is unable to comprehensively model: the turbulent mean velocity profile and the mechanism that maintains turbulence.

Empirical models have also proven useful in capturing certain aspects of turbulent flows. For example, Proper Orthogonal Decomposition (POD) has been used to construct low dimensional ordinary differential equation models of turbulent flows, see, e.g., Refs. 27 and 28. However, empirical models of this type are constructed based on data resulting from experiments or simulations rather than proceeding directly from the NS equations.

Researchers have also sought insight into turbulence through examining numerically obtained three-dimensional equilibria and periodic orbits of the NS equations, see, e.g., Refs. 29 and 30. For plane Couette flow, the first such numerical solution was computed by Nagata.[31] Details concerning these numerically obtained fixed points and periodic orbits for plane Couette flow can be found in Refs. 32 and 30. These solutions reflect local properties of the attractor and the extension of these solutions to the global turbulent dynamics has yet to be completed.

The 2D/3C model[33–35] is a recent attempt to obtain a simplified model that is nonlinear, analytically tractable and derived from the NS equations. The assumptions underlying this model are based on experimental[36–38] and analytical evidence[13,15,25,39] pointing to the central role of streamwise coherent structures in wall-turbulence. This streamwise constant model has been used to accurately simulate the mean turbulent velocity profile,[35] to identify the large-scale spanwise spacing of streamwise coherent structures and to study the energetics of fully developed turbulent plane Couette flows.[40] The primary limitation of the 2D/3C model is that it does not retain the dynamics of streamwise varying perturbations and instead relies on external excitation to generate a perturbation field. As a consequence, the 2D/3C system supports only one-way coupling, that is the perturbation field influences the mean flow but is not itself influenced by the mean flow. Moreover, the system requires persistent excitation to sustain a turbulent state. In fact, the laminar solution of the unforced 2D/3C model has been shown to be globally asymptotically stable.[41,42,69]

The current work describes a more comprehensive model that is similar to the 2D/3C model in its use of a streamwise constant mean flow, but which also incorporates two-way interaction between this streamwise constant mean flow and a streamwise varying perturbation field. This coupling is chosen to parallel that used in the Stochastic Structural Stability Theory (S3T) model.[43] The S3T equations are comprised of the joint evolution of the streamwise constant mean flow (first cumulant) and the ensemble second order perturbation statistics (second cumulant), and can be viewed as a second order closure of the dynamics of the statistical state. These equations are closed either by parameterizing the higher cumulants by a stochastic excitation[13,44,45] or by setting the third cumulant to zero, see, e.g., Refs. 46–48. This restriction of the NS equations to the first two cumulants involves parameterizing or neglecting the nonlinear interactions between the streamwise varying perturbations in the NS equations while retaining the interaction between these perturbations and the streamwise constant mean flow. This closure results in a nonlinear autonomous dynamical system that governs the evolution of the statistical state of the turbulence comprising this mean flow and its second order perturbation statistics. The restricted nonlinear (RNL) model described in the current work shares the dynamical restrictions of the S3T model but approximates the statistical closure by constructing the covariance using a single realization of the flow. In other words, a simulation of the RNL system produces the statistical state dynamics by approximating the second cumulant using a single member of the infinite ensemble that forms the covariance in the S3T dynamics.

The S3T model has recently been used to study the dynamics of fully developed wall-turbulence,[49] in particular that of the roll and streak structures. These prominent features of wall-turbulence were first identified in the buffer layer.[50] Rolls and streaks have often been suggested to play a central role in maintaining wall-turbulence. However, neither the laminar nor the turbulent streamwise mean velocity profile gives rise to these structures as a fast inflectional instability of the type generally associated with the rapid transfer of energy from the mean flow that sustains

the perturbation field. These structures are, however, associated with optimal transient growth in wall-bounded shear flows, which leads to robust transfer of energy from the mean wall-normal shear to the perturbation field. In particular, this transfer occurs as the roll circulation drives the streak perturbation through the lift-up mechanism.[51] One posited resolution of the conundrum posed by the ubiquity of the roll and streak structure in turbulence despite the linear stability of these structures, is their participation in a regeneration cycle in which the roll is maintained by perturbations resulting from the break-up of the streaks.[52,53] This proposed cycle is a nonlinear process whereby the turbulence is sustained by recurring excitation of the linear non-normal lift-up growth process.

The regeneration cycle of rolls and streaks has been attributed to a variety of alternative mechanisms collectively referred to as self-sustaining processes (SSPs). One class of SSP attributes the perturbations sustaining the roll circulation to an inflectional instability of the streak.[54–57] However, other researchers subsequently observed that most streaks in the buffer layer are too weak to support inflectional instability and postulated that transient growth is an equally plausible explanation for the origin of roll-maintaining perturbations.[58] Moreover, transiently growing perturbations can potentially tap the energy of the wall-normal mean shear. In fact, an important class of optimally growing perturbations in wall-bounded shear flows are oblique waves with this property of drawing on the mean shear[59] and consistently, oblique waves are commonly observed to accompany streaks in wall-turbulence.[58] The mechanism in which transiently growing perturbations that draw on the mean shear to maintain the roll/streak complex through a SSP requires an explicit explanation for the collocation of the perturbations with the streak, whereas SSPs based on instability of the streak inherently provide this explanation. A related SSP mechanism has been identified in the S3T system. In that SSP, which can be fully characterized using the theory of statistical state dynamics, the roll is also maintained by transiently growing perturbations that tap the energy of the mean shear rather than by an inflectional instability of the streak. The crucial departure from previously proposed transient growth mechanisms is that these transiently growing perturbations result from parametric instability of the time-dependent streak[60] rather than arising from break-down of the streak.[61] This parametric SSP explains inter alia the systematic collocation of the streak with the roll-forming perturbations and the systematic transfer of energy from the wall-normal shear to maintain the streak. The discussion above demonstrates that there remains a substantial difference of opinion among investigators as to how the nonlinear instability inherent to the conceptual model of the SSP operates. Clearly, there is a need for further investigation and new tools in order to comprehensively characterize the SSP. One such tool is provided by the RNL framework, which has a number of advantages for investigating the underlying dynamics of the SSP including its simplified dynamical setting that is directly derived from NS and easy to implement within an existing Direct Numerical Simulation (DNS). In addition, the RNL modeling framework does not rely on a particular Reynolds number or channel size to isolate the underlying mechanisms and therefore Reynolds number trends as well as the dynamics of the SSP in large channels can be explored. Another advantage of the RNL framework is that it does not model particular features of the SSP in isolation but rather captures the dynamics of these structures as part of the system dynamics.

In this paper, we first verify that the S3T dynamics are well approximated by the RNL model. We then demonstrate that the RNL system produces self-sustaining turbulence that is naturally supported by a small number of streamwise modes. Comparisons with DNS show that simulations of the RNL system produce accurate mean statistical quantities such as the mean velocity profile while supporting roll and streak structures that are consistent with those involved in the SSP of wall-turbulence. The large-scale features, perturbation energies, and spectra obtained from RNL simulations also compare favorably with those of DNS. The RNL system therefore acts as a bridge between the analytically tractable dynamics of the S3T system,[60] which can be studied using the powerful methods of matrix analysis, and DNS. Its relative analytical and computational tractability when compared to DNS along with its ability to retain essential features of wall-turbulence suggests that the RNL model and the associated S3T framework provide a powerful new platform with which to study the dynamics of wall-turbulence. For example, the severe restriction of the nonlinearity in the dynamics of the RNL together with its greatly reduced dimension may allow us to gain insight that can be used to develop flow control strategies.

The remainder of this paper is organized as follows. Section II derives the RNL model from the NS equations and establishes its relation to the S3T system. In Sec. II B we describe our numerical approach and then in Sec. III we demonstrate that the RNL system produces turbulence that is strikingly similar to that of DNS. This result verifies that the interaction between the perturbations and the streamwise constant mean flow retained in the RNL/S3T framework is sufficient for maintaining turbulent behavior. In Sec. IV we compare fully developed RNL turbulence to that arising from a stochastically forced 2D/3C model, to highlight the importance of the fundamental interactions between the perturbations and the mean flow. These interactions, which are present in the RNL model but not in the 2D/3C model, are essential for sustaining turbulence. Finally, we conclude the paper and point to directions of future study.

II. METHODS

A. Modeling framework

Consider a plane Couette flow between walls with velocities $\pm U_w$. The streamwise direction is x, the wall-normal direction is y, and the spanwise direction is z. Quantities are non-dimensionalized by the channel half-width, δ, and the wall velocity, U_w. The non-dimensional lengths of the channel in the streamwise and spanwise directions are, respectively, L_x and L_z. Streamwise averaged, spanwise averaged, and time averaged quantities are, respectively, denoted by angled brackets, $\langle \bullet \rangle = \frac{1}{L_x} \int_0^{L_x} \bullet \, dx$, square brackets, $[\bullet] = \frac{1}{L_z} \int_0^{L_z} \bullet \, dz$, and an overline $\overline{\bullet} = \frac{1}{T} \int_0^T \bullet \, dt$, with T sufficiently large. The velocity field $\mathbf{u}_T$ is decomposed into its streamwise mean, $\mathbf{U}(y, z, t) = (U, V, W)$, and the deviation from this mean (the perturbation), $\mathbf{u}(x, y, z, t) = (u, v, w)$. The pressure gradient is similarly decomposed into its streamwise mean, $\nabla P(y, z, t)$, and the deviation from this mean, $\nabla p(x, y, z, t)$. The corresponding Navier-Stokes (NS) equations are

$$\mathbf{U}_t + \mathbf{U} \cdot \nabla \mathbf{U} + \nabla P - \frac{1}{R} \Delta \mathbf{U} = -\langle \mathbf{u} \cdot \nabla \mathbf{u} \rangle, \tag{1a}$$

$$\mathbf{u}_t + \mathbf{U} \cdot \nabla \mathbf{u} + \mathbf{u} \cdot \nabla \mathbf{U} + \nabla p - \frac{1}{R} \Delta \mathbf{u} = -(\mathbf{u} \cdot \nabla \mathbf{u} - \langle \mathbf{u} \cdot \nabla \mathbf{u} \rangle) + \epsilon, \tag{1b}$$

$$\nabla \cdot \mathbf{U} = 0, \ \nabla \cdot \mathbf{u} = 0, \tag{1c}$$

where the Reynolds number is defined as $R = U_w \delta / \nu$, with kinematic viscosity ν. The parameter ϵ in (1b) is an externally imposed divergence-free stochastic excitation that is used to induce transition to turbulence.

We derive the RNL system from (1) by first introducing a stochastic excitation, $\mathbf{e}$, to parameterize the nonlinearity, $\mathbf{u} \cdot \nabla \mathbf{u} - \langle \mathbf{u} \cdot \nabla \mathbf{u} \rangle$ as well as divergence-free external excitation ϵ in (1b) to obtain

$$\mathbf{U}_t + \mathbf{U} \cdot \nabla \mathbf{U} + \nabla P - \frac{1}{R} \Delta \mathbf{U} = -\langle \mathbf{u} \cdot \nabla \mathbf{u} \rangle, \tag{2a}$$

$$\mathbf{u}_t + \mathbf{U} \cdot \nabla \mathbf{u} + \mathbf{u} \cdot \nabla \mathbf{U} + \nabla p - \frac{1}{R} \Delta \mathbf{u} = \mathbf{e}, \tag{2b}$$

$$\nabla \cdot \mathbf{U} = 0, \ \nabla \cdot \mathbf{u} = 0. \tag{2c}$$

This results in a nonlinear system where (2a) describes the dynamics of a streamwise mean flow driven by the divergence of the streamwise averaged Reynolds stresses; we denote these streamwise averaged perturbation Reynolds stress components as, e.g., $\langle uu \rangle$, $\langle uv \rangle$. On the other hand, Eq. (2b) accounts for the interactions between the streamwise varying perturbations, $\mathbf{u}(x, y, z, t)$, and the streamwise constant mean flow, $\mathbf{U}(y, z, t)$. Equation (2b) can be linearized around $\mathbf{U}(y, z, t)$ to yield

$$\mathbf{u}_t = A(\mathbf{U})\mathbf{u} + \mathbf{e}, \tag{3}$$

where $A(\mathbf{U})$ is the associated linear operator, which is described in detail in the Appendix.

The closely related S3T system is obtained by making the ergodic assumption of equating the streamwise average with the ensemble average over realizations of the stochastic excitation ϵ in (1b). The S3T system is then formed as a second order closure of the NS equations in (1), in which the first order cumulant is **U** and the second order cumulant is the corresponding spatial covariance C between any two points $\mathbf{x}_1$ and $\mathbf{x}_2$. We refer to the resulting closed system of equations as the (second order) statistical state dynamics of the flow:

$$\mathbf{U}_t = -\mathbf{U} \cdot \nabla \mathbf{U} - \nabla \mathbf{P} + \frac{1}{R}\Delta \mathbf{U} + \mathcal{L}C, \tag{4a}$$

$$C_t = (A_1(\mathbf{U}) + A_2(\mathbf{U}))\,C + Q. \tag{4b}$$

Here, Q is the second order covariance of the stochastic excitation, which is assumed to be temporally delta correlated, and $\mathcal{L}C$ denotes the divergence of the streamwise averaged Reynolds stresses expressed as a linear function of the covariance C. The expression $\mathbf{A}_1(\mathbf{U})C$ accounts for the contribution to the time rate of change of the covariance arising from the action of the operator $A(\mathbf{U})$ evaluated at point $\mathbf{x}_1$ on the corresponding component of C. A similar relation holds for $\mathbf{A}_2(\mathbf{U})C$. Further details regarding Eqs. (3) and (4) are provided in the Appendix.

In isolation, the mean flow dynamics (4a) define a streamwise constant or 2D/3C model of the flow field[35, 41] forced by the divergence of the streamwise averaged Reynolds stresses specified by $\mathcal{L}C$. The S3T system (4) describes the statistical state dynamics closed at second order, which has been shown to be sufficiently comprehensive to allow identification of statistical equilibria of turbulent flows and permit analysis of their stability.[60] The S3T system provides an attractive theoretical framework for studying turbulence through analysis of its underlying statistical mean state dynamics. However, it has the perturbation covariance as a variable and as a result becomes computationally intractable for high dimensional systems. In particular, the perturbation covariance has dimension $O(N^2)$ for a system of dimension $O(N)$ and is only directly integrable for low order systems.

The RNL model shares the dynamical restrictions of the S3T model and these systems can therefore be directly related to one another. Results obtained from the RNL and S3T models will agree if the exact covariance of the S3T is adequately approximated by the single ensemble member retained in the RNL model. Since the RNL model in (2) uses a single realization to approximate the ensemble covariance rather than employ the infinite ensemble of the S3T dynamics, it avoids explicit time integration of the perturbation covariance equation and therefore facilitates computationally efficient studies of the S3T system dynamics. The RNL system has the additional advantage that it can be easily implemented by restricting a DNS code to the RNL dynamics in (2).

In this paper we consider the unforced RNL system, which corresponds to setting $\mathbf{e} = 0$ in (2b). This system models the RNL dynamics occurring after an initial transient phase during which an excitation has been applied to initiate turbulence. We demonstrate that subsequent to this transient phase, the RNL system supports turbulence that closely resembles a DNS of fully developed turbulence in plane Couette flow.

B. Numerical method

The numerical simulations in this paper were carried out using a spectral code based on the Channelflow NS equations solver.[62, 63] The time integration uses a third order multistep semi-implicit Adams-Bashforth/backward-differentiation scheme that is detailed in Ref. 64. The discretization time step is automatically adjusted such that the Courant-Friedrichs-Lewy (CFL) number is kept between 0.05 and 0.2. The spatial derivatives employ Chebyshev polynomials in the wall-normal (y) direction and Fourier series expansions in the streamwise (x) and spanwise (z) directions.[65] No-slip boundary conditions are employed at the walls for the y component and periodic boundary conditions are used in the x and z directions for all of the velocity fields. Aliasing errors from the Fourier transforms are removed using the 3/2-rule, as detailed in Ref. 66. A zero pressure gradient is imposed in all simulations. Table I provides the dimensions of the computational box, the number of

TABLE I. Geometry for the numerical simulations. x, y, and z define the computational domain. N_x, N_y, and N_z are the number of grid points in their respective directions. M_x and M_z are the number of respective x and z Fourier modes used after dealiasing and M_y is the number of Chebyshev modes used in each simulation.

	x	y	z	$N_x \times N_y \times N_z$	$M_x \times M_y \times M_z$
DNS	$[0, 4\pi]$	$[-1, 1]$	$[0, 4\pi]$	$128 \times 65 \times 128$	$83 \times 65 \times 41$
RNL	$[0, 4\pi]$	$[-1, 1]$	$[0, 4\pi]$	$16 \times 65 \times 128$	$9 \times 65 \times 41$
2D/3C		$[-1, 1]$	$[0, 4\pi]$	65×128	65×41

grid points, and the number of spectral modes for the DNS and simulations of the RNL and 2D/3C systems.

In both the DNS and RNL simulations we use the respective stochastic excitations ϵ in (1) and **e** in (2) only to initiate turbulence. In order to perform the RNL computations the DNS code was restricted to the dynamics of (2) with **e** = 0.

For simulations of the 2D/3C system, the influence of the instantaneous mean flow $\mathbf{U}(y, z, t)$ on the perturbation dynamics was eliminated by replacing the term $\mathbf{U} \cdot \nabla \mathbf{u} + \mathbf{u} \cdot \nabla \mathbf{U}$ on the right-hand side of (2b) with $\mathbf{U_{lam}} \cdot \nabla \mathbf{u} + \mathbf{u} \cdot \nabla \mathbf{U_{lam}}$, where $\mathbf{U_{lam}} = (U(y), 0, 0)$ defines the laminar velocity profile for plane Couette flow with $U(y) = y$.

III. RESULTS

In this section we compare simulations of the RNL system (2) to DNS of fully developed turbulence in plane Couette flow. Turbulence is initiated by applying the stochastic excitation ϵ in (1b) for the DNS cases and **e** in (2b) for the RNL simulations over the interval $t \in [0, 500]$, where t represents convective time units. All of the averaged quantities reported are for $t > 1000$ and all of the results in this section are based on $R = 1000$. The geometry and resolution for each of the DNS and RNL cases in this section are given in Table I. This table reflects one of the computational benefits of the RNL system: the fact that its turbulence is supported by a greatly reduced number of streamwise modes. This reduction in the dimension of the dynamics supporting the turbulent state in the RNL system is not a restriction of the dynamics but rather a direct consequence of the modeling framework, and is consistent with the similar reduced number of streamwise modes that supports turbulence in the S3T system as discussed in Ref. 60. We verified that increasing the number of streamwise modes used for the RNL simulations has no effect on the simulation results reported herein.

The turbulent mean velocity profile obtained from the DNS is compared to that obtained using the unforced RNL system in Figure 1(a). Figure 1(b) provides a comparison of the same data in wall units, $u^+ = u/u_\tau$ and $y^+ = (y + 1)u_\tau/\nu$ with friction velocity $u_\tau = \sqrt{\tau_w/\rho}$, $Re_\tau = u_\tau \delta/\nu$, and $\nu = 1/R$. The wall unit values for the DNS data shown in Figure 1(b) are $Re_\tau = 66.2$ and $u_\tau/U_w = 6.62 \times 10^{-2}$, while the corresponding parameters for the RNL simulation are $Re_\tau = 64.9$ and $u_\tau/U_w = 6.49 \times 10^{-2}$. Figure 1 illustrates good agreement between the turbulent mean velocity profile obtained from the RNL simulation and that obtained from the DNS, which is consistent with recent studies.[49,67]

Instantaneous snapshots of the turbulent velocity fields from the DNS and the RNL simulation are displayed in Figure 2, which shows contour plots of the U velocity field with the V, W vector fields superimposed. The particular snapshots shown in Figure 2 suggest that the DNS and the RNL system produce similar roll circulations and streak structures. We investigate the similarity of the streaks arising from the DNS and the RNL simulation further in Figures 3(a) and 3(b), which, respectively, show the spectral densities of the streak velocity, $U - [U]$, at $y^+ = 15$ and the center of the channel. The reported values are averaged over 1000 convective time steps. The spectral densities of the streaks obtained from the RNL simulation and the DNS at $y^+ = 15$ have nearly the same peak energy density, which occurs at a wavelength of $4\pi/3\delta$. At this wall normal location, the energy density of the streaks in both systems sharply decay at longer wavelengths. At the channel center, the RNL simulation and DNS agree well at low wave numbers and show similar trends.
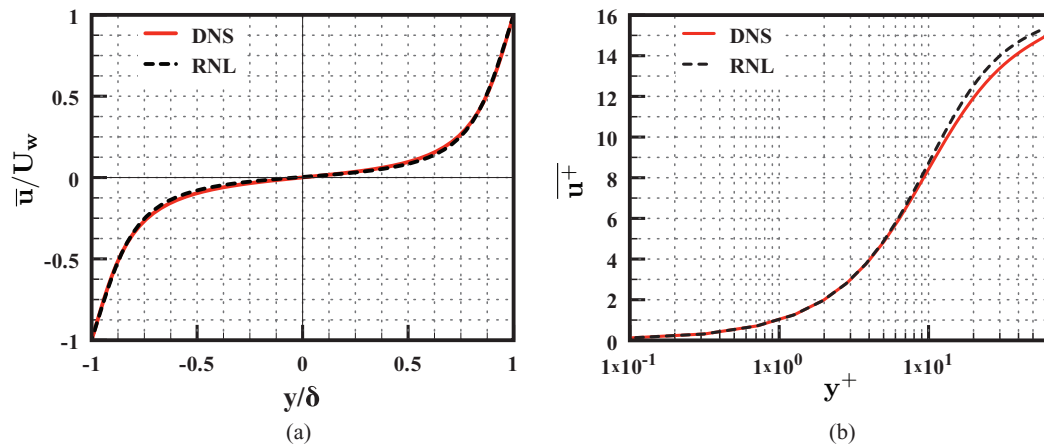
FIG. 1. Turbulent mean velocity profiles (based on streamwise, spanwise, and time averages) in (a) geometric units and (b) wall units obtained from the DNS (red solid line) and the RNL simulation (black dashed line).

However, the streak energy density of the DNS attains a higher peak. The streak energy density of the RNL system also shows a broader peak that occurs over $\lambda_z \in [2\pi, 4\pi]\delta$ versus $\lambda_z \in [2\pi, 4\pi/3]\delta$ in the DNS. The results in Figure 3 show close agreement between the spectral density of the DNS and RNL system streaks in the near wall region and only modest differences at the center of the channel.
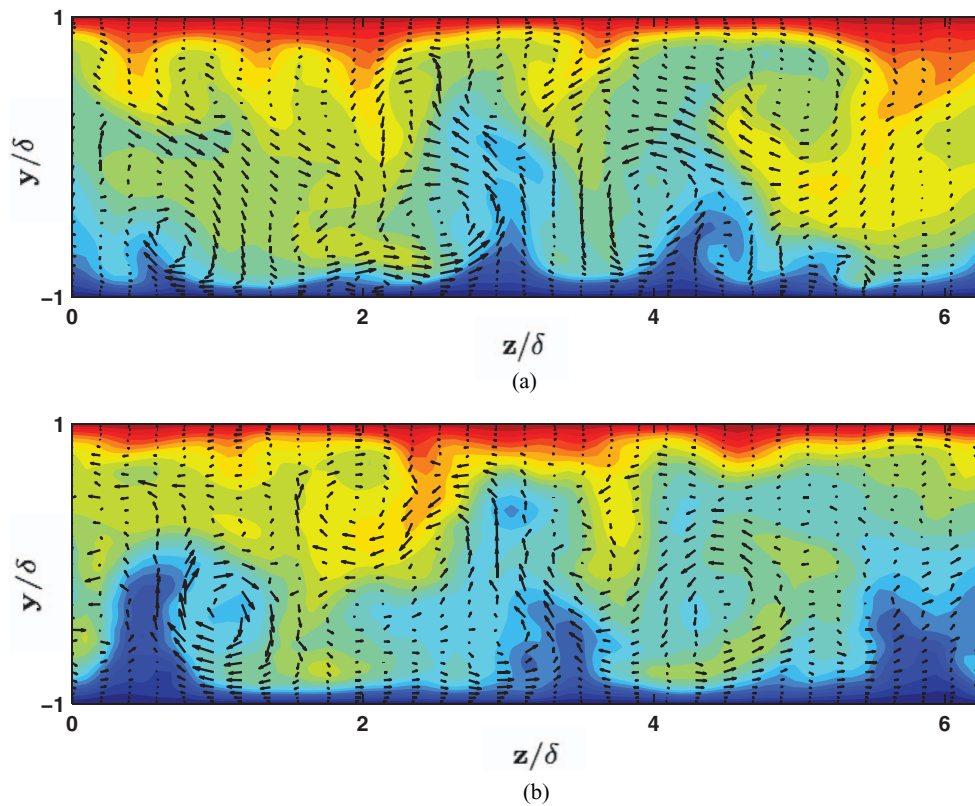
FIG. 2. A y-z plane cross-section of the flow (at $x = 0$) at a single snapshot in time for the (a) DNS and the (b) RNL simulation. Both panels show contours of the streamwise component of the flow, u_T, with the wall-normal and spanwise velocity vectors superimposed. The RNL is self-sustaining ($\mathbf{e} = 0$) for the time shown. (a) DNS, (b) RNL.
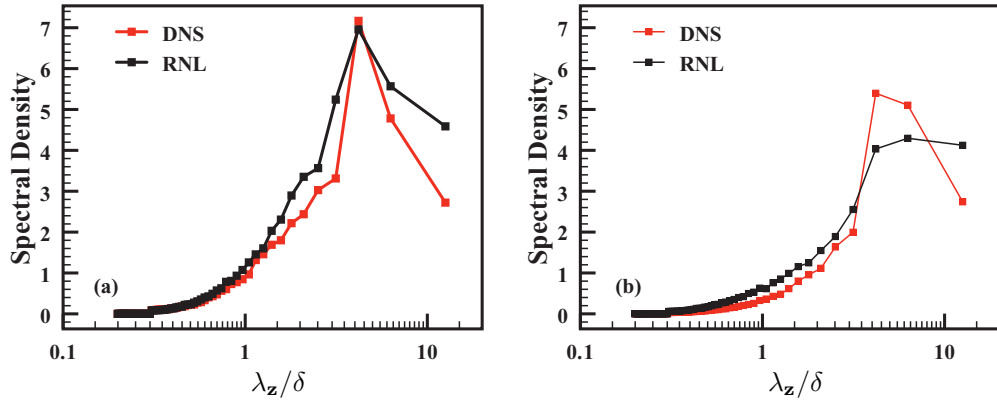
FIG. 3. Averaged spectral densities of the streak velocity, $U - [U]$, at (a) the center of the channel and (b) $y^+ = 15$. Each panel compares the RNL simulation (black squares) to the DNS (red squares). Lines are shown solely to guide the eye. (a) $\mathbf{y}^+ = 15$, (b) channel center.

Figure 4 shows the spanwise premultiplied spectra, $k_z E_i(\tilde{y}, \lambda_z)$ for the RNL simulation and the DNS. Here we define the spanwise premultiplied spectra as

$$k_z E_i(\tilde{y}, \lambda_z) = k_z \frac{\sum_{k_x} E_{ii}(\tilde{y}, k_x, k_z)}{\sum_{\tilde{y}} \sum_{k_x} E_{ii}(\tilde{y}, k_x, k_z)}, \tag{5a}$$

$$E_{ii}(\tilde{y}, k_x, k_z) = \hat{i}(\tilde{y}, k_x, k_z)\, \hat{i}^\dagger(\tilde{y}, k_x, k_z), \tag{5b}$$

where $\lambda_z = L_z/k_z$, $\tilde{y} = y + 1$, $i \in \{u, v, w\}$, $\hat{i}$ is the Fourier transform of i with respect to x and z, and $\hat{i}^\dagger$ is the complex conjugate of $\hat{i}$. The premultiplied spectra of both the DNS and the RNL simulation exhibit a shift from longer wavelengths far from the wall to smaller wavelengths closer to the wall. The results for $k_z E_v(\tilde{y}, \lambda_z)$ and $k_z E_w(\tilde{y}, \lambda_z)$ show modest differences, in particular the
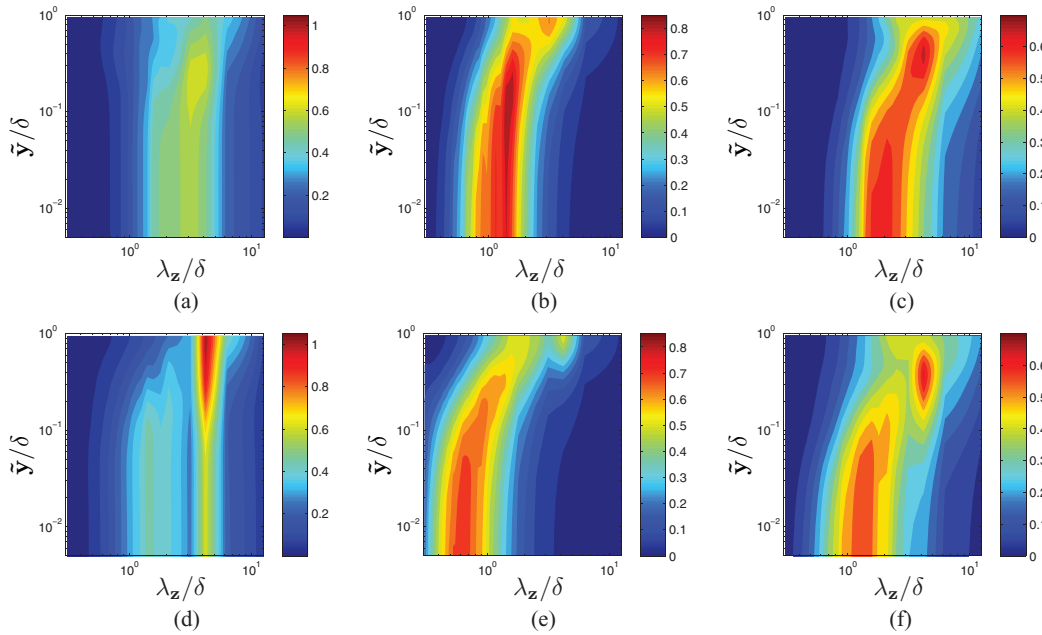

FIG. 4. Normalized premultiplied spectra $k_z E_i(\tilde{y}, \lambda_z)$ for $i = \{u, v, w\}$ as a function of spanwise wavelength, λ_z/δ, and $\tilde{y}/\delta$, where $\tilde{y} = y + 1$. Panels (a)–(c) respectively show $k_z E_u(\tilde{y}, \lambda_z)$, $k_z E_v(\tilde{y}, \lambda_z)$, and $k_z E_w(\tilde{y}, \lambda_z)$ from the RNL simulation. Panels (d)–(f) show the same quantities computed from the DNS.
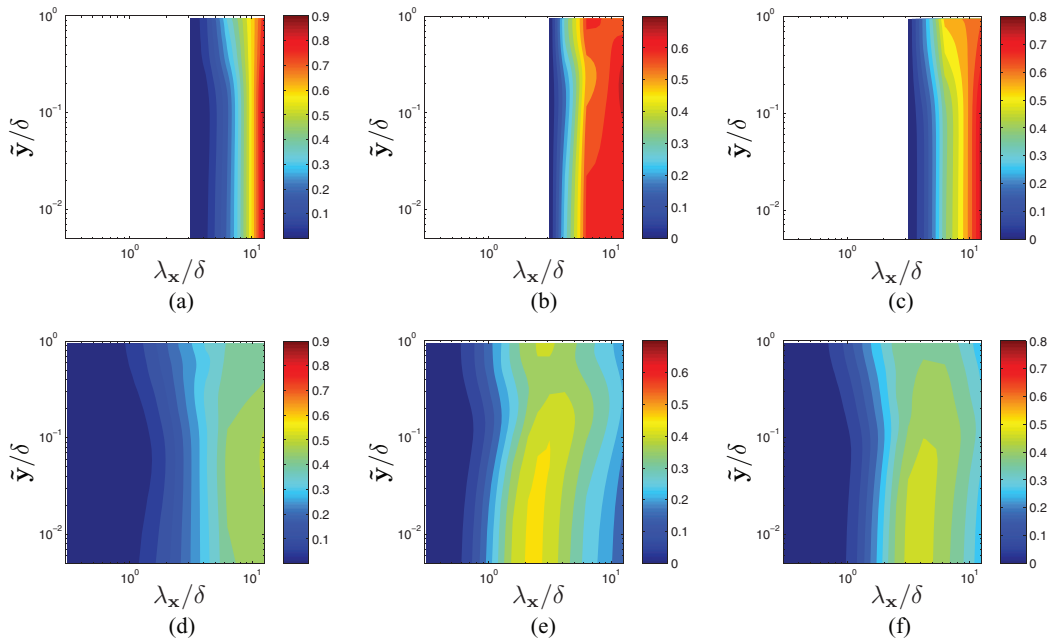
FIG. 5. Normalized premultiplied spectra $k_x E_i(\tilde{y}, \lambda_x)$ for $i = \{u, v, w\}$ as a function of streamwise wave length, λ_x/δ, and $\tilde{y}/\delta$, where $\tilde{y} = y + 1$. Panels (a)–(c) respectively show $k_x E_u(\tilde{y}, \lambda_x)$, $k_x E_v(\tilde{y}, \lambda_x)$, and $k_x E_w(\tilde{y}, \lambda_x)$ from the RNL simulation. Panels (d)–(f) show the same quantities for the DNS. The RNL premultiplied spectra exhibit a rapid falloff in streamwise energies in comparison to the DNS premultiplied spectra.

peaks of these spectra occur at a smaller spanwise wavelength in the DNS data versus the RNL results. This reflects a mildly steeper falloff in the energy associated with the small scales in the DNS as compared to the RNL system. The $k_z E_u(\tilde{y}, \lambda_z)$ values for the DNS shown in Figure 4(d) have a pronounced bimodality and localized concentration of the spanwise premultiplied spectra around a small interval of spanwise wavelengths. These features are not seen in the RNL results in Figure 4(a) and this difference is the subject of ongoing work.

Figure 5 shows the corresponding streamwise premultiplied spectra, calculated in a manner consistent with (5). Here, the effect of the reduced number of streamwise modes that are supported by the RNL system dynamics is clear. The concentration of these spectra in the largest scales results directly from setting $\mathbf{e} = 0$ in (2b). When this is done, all but a small number of the streamwise modal energies in the RNL vanish rapidly, i.e., when $\mathbf{e} = 0$ the RNL system is naturally supported by a small number of streamwise harmonics. Consequently, the RNL model can be explored using simulations with a very small number of streamwise modes. The practical application of this result is made clear in Table I, which shows that only 16 streamwise modes are needed to calculate the RNL model as opposed to 128 streamwise modes for the DNS.

Figure 6 shows the time-averaged Reynolds stresses, $[\overline{\langle u'^+ u'^+ \rangle}]$, $[\overline{\langle u'^+ v'^+ \rangle}]$, $[\overline{\langle v'^+ v'^+ \rangle}]$, and $[\overline{\langle w'^+ w'^+ \rangle}]$ where the streamwise fluctuations, u', are defined as $u' = u_T - \overline{u_T}$, the wall-normal fluctuations, v', are defined as $v' = v_T - \overline{v_T}$ and the spanwise fluctuations, w', are defined as $w' = w_T - \overline{w_T}$. u'^+, v'^+, and w'^+ designate these fluctuations scaled by u_τ, such that $u'^+ = u'/u_\tau$, $v'^+ = v'/u_\tau$, and $w'^+ = w'/u_\tau$. These figures illustrate close agreement between the $\overline{u'v'}$ Reynolds stress obtained from the RNL simulation and DNS. As shown in Figure 1(b), the turbulent flow supported by DNS and the RNL simulation exhibit nearly identical shear at the boundary. Therefore, the average energy input and by consistency the dissipation must be the same in these simulations. On the other hand, the streamwise component of the time-averaged Reynolds stresses, $\overline{u'u'}$, attains a higher peak magnitude in the RNL simulation than in the DNS. This difference is not surprising because the streamwise varying components are substantially influenced by interactions with small scales in the flow. The nonlinear interactions between the streamwise varying perturbations that are neglected by the RNL model participate in the transfer of energy to the small scales of the flow
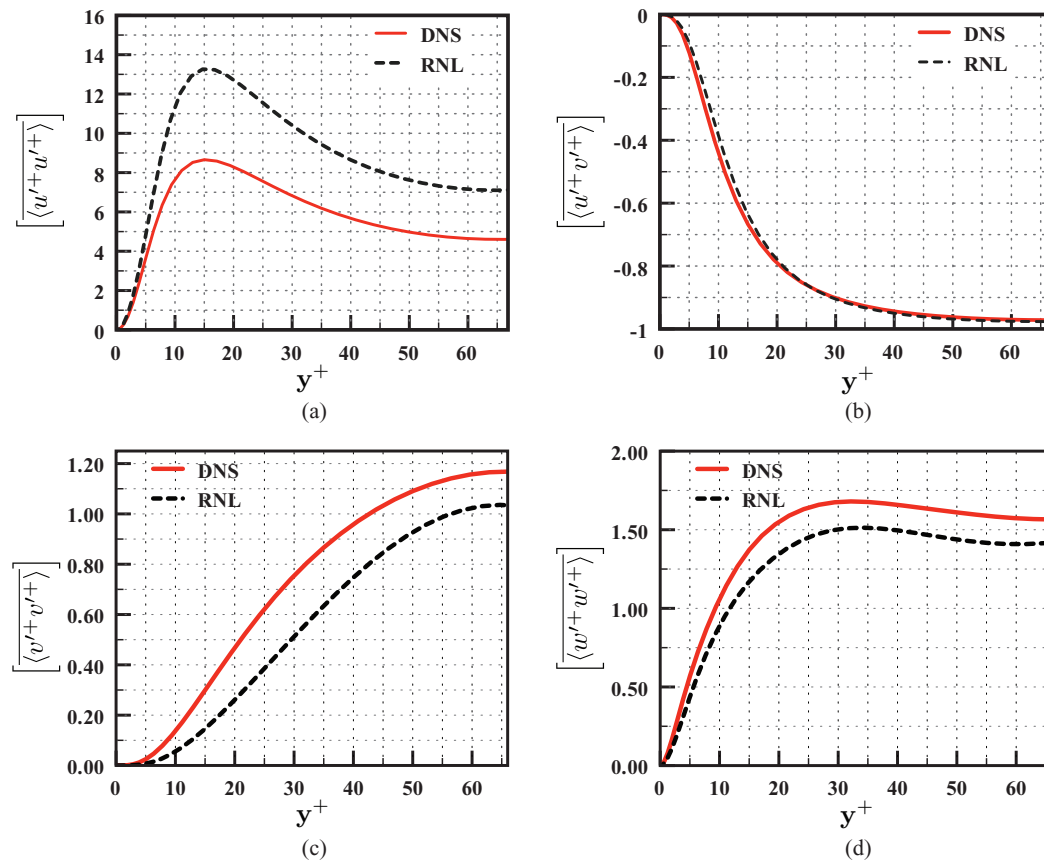
FIG. 6. Time-averaged Reynolds stresses (a) $[\overline{\langle u'^+u'^+\rangle}]$, (b) $[\overline{\langle u'^+v'^+\rangle}]$, (c) $[\overline{\langle v'^+v'^+\rangle}]$ and (d) $[\overline{\langle w'^+w'^+\rangle}]$ obtained from the DNS (red solid line) and the RNL simulation (black dashed line).

and removing these interactions leads to the elimination of flow energy associated with higher wave numbers. As a result, there is substantially reduced effective perturbation induced dissipation of the supported lower wave number fluctuations. Under this curtailment of spectral transfer, the associated time-averaged streamwise normal Reynolds stress attains a larger magnitude at equilibrium in the RNL system. In contrast, the wall-normal and spanwise time-averaged Reynolds stress components have a lower magnitude in the RNL model as compared to the DNS. This indicates that the Reynolds stresses required to maintain the RNL mean velocity profile at statistical equilibrium are being produced by smaller RMS amplitudes for the v' and w' velocity components. Further characterization of these differences and the related dynamics are the subject of continuing investigation.

Figures 7(a), 8(a), and 9(a), respectively show close agreement in the root-mean-square (RMS) velocity departure from laminar, defined as $\sqrt{(\mathbf{u}_T - \mathbf{U}_{\mathrm{lam}})^2}$, the RMS streak velocity, $\sqrt{(U - [U])^2}$, and the RMS roll velocity, $\sqrt{V^2 + W^2}$, obtained from the RNL simulation and the DNS. Although these values are reported over the time interval $t \in [200, 2000]$, the behavior remains consistent over longer time periods and when different time intervals are selected. The fact that the RNL system produces self-sustaining turbulence is demonstrated in these figures as the system maintains the same behavior after the initial forcing is removed (i.e., there are no differences observed between the behavior before and after $t = 500$).

The time scales associated with the RMS of the velocity deviation from laminar, the RMS streak velocity, and the RMS roll velocity are explored in Figures 7(b), 8(b), and 9(b), which display the temporal Fourier spectra associated with these quantities calculated over the time interval $t \in [1000, 6000]$. These plots show close agreement in the time-scales of these quantities especially in the RMS of the velocity departure from laminar and the RMS streak. The RMS roll spectrum has
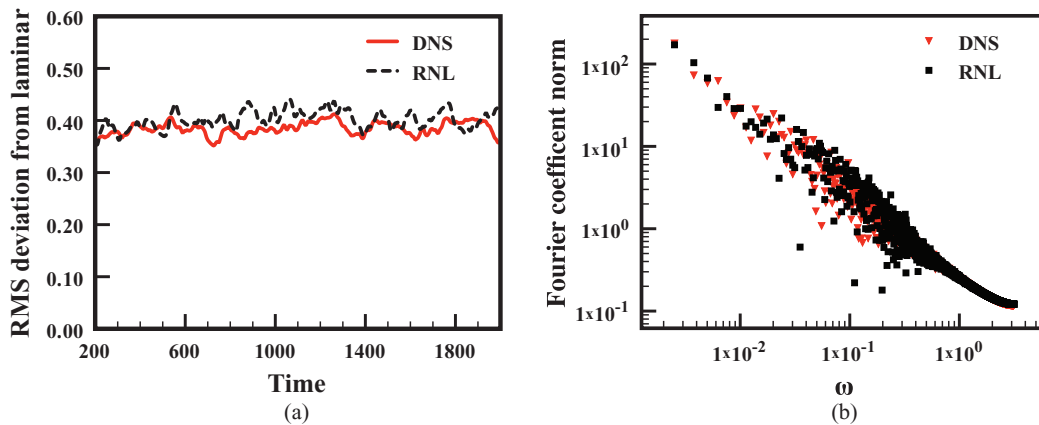
FIG. 7. (a) RMS of the velocity deviation from laminar, $\sqrt{(\mathbf{u}_T - \mathbf{U}_{\mathbf{lam}})^2}$ versus time for the DNS (red solid line) and the RNL simulation (black dashed line) and (b) the corresponding Fourier spectrum for the DNS (red triangles) and the RNL simulation (black squares).

a higher amplitude than the DNS, especially in the energy associated with the longest scales. This difference is the topic of ongoing study. The close correspondence between the RNL simulation and the DNS in the quantities depicted in Figures 7–9 indicates that the RNL system accurately captures important structural features of turbulence despite its dynamical restrictions. These results also indicate strong similarities between the structural features of the rolls and streaks in RNL turbulence and the roll/streak structures that play a key role in the SSP identified in the S3T model.[60] This observation combined with the close relationship between the S3T and RNL dynamics suggest that these SSPs share an underlying mechanism. Further investigations of these similarities is the subject of ongoing work.

Figure 10(a) shows Re_τ from the RNL simulation and the DNS as a function of dimensionless time, $u_\tau t/\delta$. The time interval in Figure 10(a) corresponds to $t \in [1000, 6000]$, which verifies that the RNL system maintains turbulence over an extended interval of time. The RNL simulation thus exhibits both self-sustaining behavior and dissipation comparable to that of DNS. Figure 10(b) compares the temporal Fourier spectrum of Re_τ of the RNL simulation and the DNS. This calculation used the convective time t rather than the dimensionless time, $u_\tau t/\delta$ reported in Figure 10(a). As with the spectra of the velocity measures reported in Figures 7(b), 8(b), and 9(b), the Fourier spectrum of Re_τ shows that the RNL system and DNS have similar temporal behaviors.
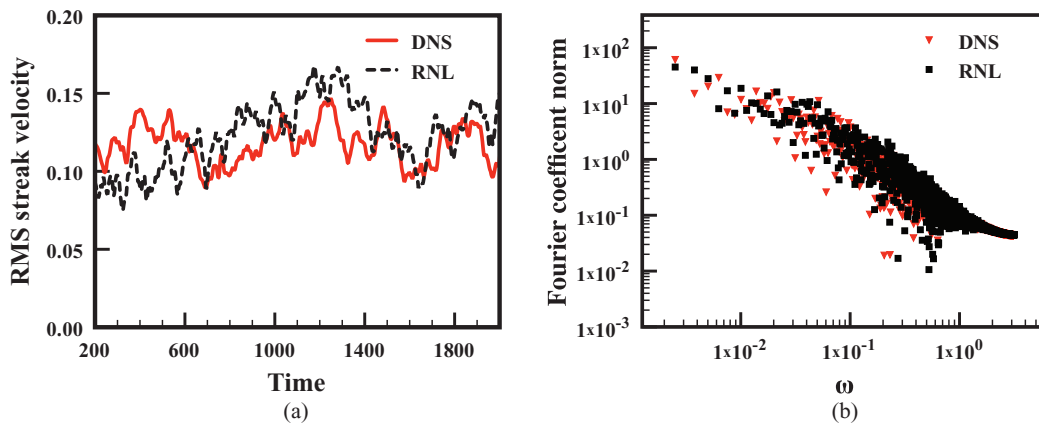

FIG. 8. (a) RMS streak velocity, $\sqrt{(U - [U])^2}$ versus time for the DNS (red solid line) and the RNL simulation (black dashed line) and (b) the corresponding Fourier spectrum for the DNS (red triangles) and the RNL simulation (black squares).
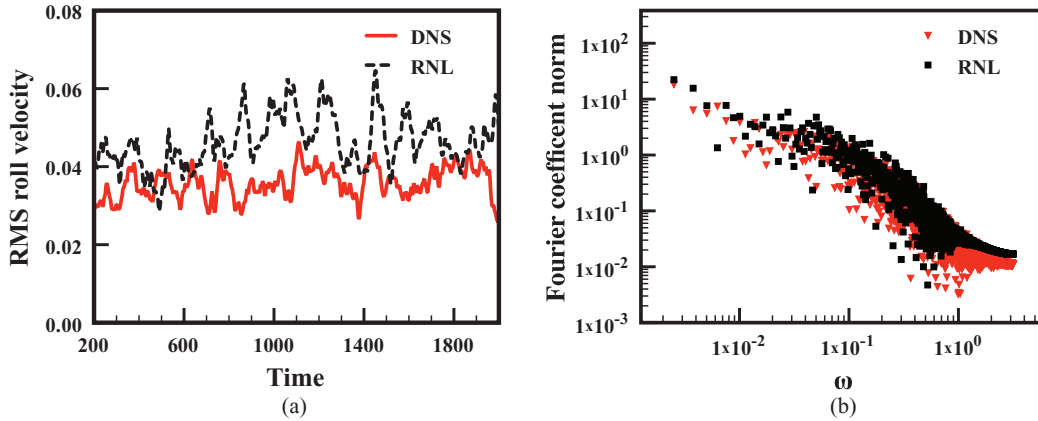
FIG. 9. (a) RMS roll velocity, $\sqrt{V^2 + W^2}$ versus time for the DNS (red solid line) and the RNL simulation (black dashed line) and (b) the corresponding Fourier spectrum for the DNS (red triangles) and the RNL simulation (black squares).
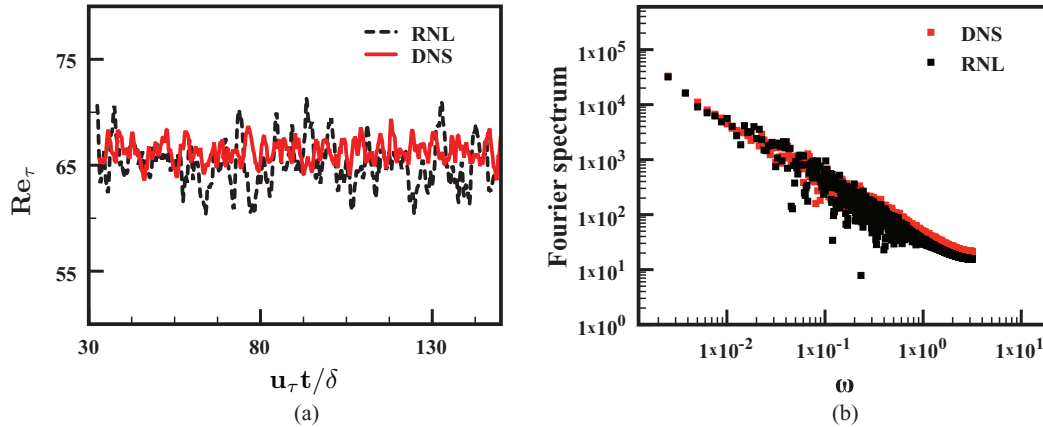

FIG. 10. (a) Re_τ versus dimensionless time, $u_\tau t/\delta$ obtained from the DNS (red solid line) and the RNL simulation (black dashed line) and (b) Fourier spectrum of the time evolution of Re_τ for the DNS (red triangles) and the RNL simulation (black squares). This Fourier spectrum is calculated for Re_τ versus the convective time scale, t, as opposed to the dimensionless time parameter, $u_\tau t/\delta$, used in (a). The time-averaged values corresponding to the DNS data are $Re_\tau = 66.2$ and $u_\tau/U_w = 6.62 \times 10^{-2}$. The corresponding values for the RNL simulation are $Re_\tau = 64.9$ and $u_\tau/U_w = 6.49 \times 10^{-2}$.

IV. COMPARISON OF THE RNL AND 2D/3C MODELS

We now verify the fundamental role of the coupling between the mean flow equation (2a) and the perturbation equation (2b) in the maintenance of turbulence in the RNL system by comparing the RNL and 2D/3C models.[35] The 2D/3C system can be obtained from (4) by replacing the instantaneous mean flow $\mathbf{U}(y, z, t)$ in (4b) with the laminar Couette flow $\mathbf{U_{lam}} = U(y)$ in order to eliminate the interaction whereby the mean flow influences the perturbations. In this case, we can express the mean flow dynamics as a forced streamwise constant (2D/3C) system given by

$$\mathbf{U}_t + \mathbf{U} \cdot \nabla \mathbf{U} + \nabla \mathbf{P} - \frac{1}{R}\Delta\mathbf{U} = \mathcal{L}C^\infty, \tag{6a}$$

$$(A_1(\mathbf{U}_{lam}) + A_2(\mathbf{U}_{lam}))\, C^\infty = -Q, \tag{6b}$$

where C^∞ denotes the asymptotic equilibrium of the perturbation covariance and Q is the second order covariance of a spatially (in y and z) and temporally delta-correlated, divergence free stochastic excitation, that is, Tukey filtered to match the boundary conditions, see, e.g., Ref. 49.

Figure 11(a) shows the same mean velocity profiles as in Figure 1(a) along with one obtained using a stochastically forced 2D/3C model.[35] This plot demonstrates close correspondence between
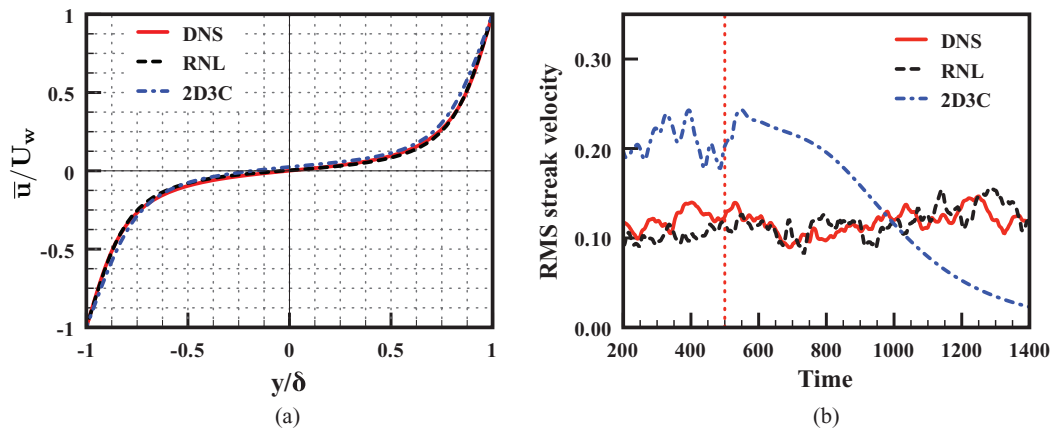
FIG. 11. (a) Turbulent mean velocity profiles (based on a streamwise, spanwise, and time averages) obtained from the DNS (red solid line), and simulations of the RNL (black dashed line) and 2D/3C systems (blue dashed-dotted line). There is no stochastic excitation applied to the DNS or the RNL simulation during the time interval used to generate the profile, whereas the 2D/3C simulation was continuously forced with $e = 0.030$. (b) The RMS streak velocity $\sqrt{(U - [U])^2}$ obtained from the DNS (red solid line) as well as the RNL (black dashed line) and 2D/3C simulations (blue dashed-dotted line) where stochastic excitation was applied to each model for $t \in [0, 500]$, i.e., the excitation was stopped at $t = 500$, which is indicated by the vertical red dotted line.

the mean velocity profiles obtained from DNS and simulations of the 2D/3C and RNL systems. Figure 11(b) shows the time evolution of the RMS streak velocity from the DNS as well as that from the 2D/3C and RNL simulations. This figure shows that the streak in the 2D/3C model gradually decays to zero after the external excitation is removed at $t = 500$. These results demonstrate that a stochastically forced 2D/3C model accurately captures the turbulent mean flow profile, but cannot maintain turbulence without persistent excitation, see, e.g., Refs. 41, 69.

   The critical difference between the 2D/3C and RNL systems is that the 2D/3C model lacks two-way interaction between the mean flow (2a) and the perturbation dynamics (2b). This difference is summarized by the block diagram in Figure 12. Both of these models include pathway ① in which the perturbations, $\mathbf{u}(\mathbf{x}, \mathbf{y}, \mathbf{z}, \mathbf{t})$, influence the dynamics of the mean flow, $\mathbf{U}(\mathbf{y}, \mathbf{z}, \mathbf{t})$. However, the RNL system (and its associated ensemble mean S3T model) also includes the feedback pathway ②, from the mean flow to the perturbation dynamics. In Figure 11(b) the effect of this feedback from the mean flow to the perturbations, pathway ② in Figure 12, is seen to be critical for capturing the mechanism of the SSP maintaining the turbulent state. As shown in Sec. III and in Figure 11, turbulence in the RNL system self-sustains (i.e., is maintained in the absence of stochastic excitation). Turbulence maintained by the same mechanism was seen previously in the S3T system in a minimal channel study.[60]
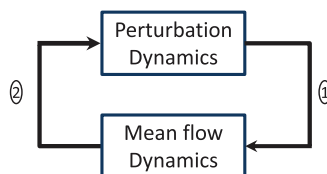

FIG. 12. In both the 2D/3C and the unforced RNL model (II A) (and its associated ensemble mean S3T model) the perturbations, $\mathbf{u}$, influence the dynamics of the mean flow, $\mathbf{U}$. This coupling is denoted pathway ① in the block diagram. The RNL and S3T models augment the 2D/3C formulation with feedback from the mean flow to the perturbation dynamics, which is illustrated through pathway ②.

In addition to being necessary to produce self-sustaining turbulence, the feedback from the mean flow to the perturbations produces streaks that are quantitatively and qualitatively similar to those observed in the DNS results, and notably more accurate than those obtained in the 2D/3C simulation. This result is consistent with the fact that in the 2D/3C model the streak is not regulated by feedback from the mean flow to the perturbation field, pathway ② in Figure 12. Therefore, understanding the maintenance of the roll and streak structures as well as the mechanism by which turbulence is maintained in a statistical steady state requires a model that includes feedback from the streamwise constant mean flow to the streamwise varying perturbation dynamics. Remarkably, only this additional feedback needs to be added to the 2D/3C system to capture the dynamics of the SSP, that is to both maintain the turbulent state and enforce its statistical equilibrium.

V. CONCLUSIONS AND DIRECTIONS FOR FUTURE WORK

In this work we have demonstrated that the RNL system, which adopts the dynamical restrictions of the S3T model, self-sustains turbulent activity. Comparisons between RNL simulations and DNS demonstrate good agreement between the mean velocity fields and the dynamically central $[\overline{\langle u'^+ v'^+ \rangle}]$ component of the time-averaged Reynolds stress, while quantitative differences in the normal Reynolds stress components are seen. The results of this work suggest that the maintenance of turbulence is crucially related both to the influence of the perturbations on the streamwise mean flow (captured in the forced 2D/3C model) and the feedback from the mean flow to the streamwise varying perturbation field, which is additionally retained in the RNL model. Given that the RNL system restricts nonlinearity to the mean flow equations and nonlinear coupling to that between the streamwise mean flow components and the perturbations, this agreement indicates that this highly restricted dynamics captures the fundamental mechanism sustaining turbulence in plane Couette flow. The ability to capture self-sustaining turbulence in a computationally and analytically tractable framework opens up new avenues for probing the dynamics of wall-turbulence and developing flow control strategies. The insight gained through this restricted model can then be tested in DNS.

The RNL model shares the dynamical restriction of the S3T system and can be obtained directly from a DNS by eliminating the streamwise varying perturbation-perturbation nonlinearity while retaining the streamwise constant mean-perturbation nonlinearities. The results of this work demonstrate that S3T dynamics are well approximated by the single realization of the S3T covariance used in the RNL model. The RNL system can therefore be seen as providing a bridge between the S3T model and DNS, which allows analytic insights gained using the S3T model to be related to DNS and for the mechanisms operating in these systems to be comprehensively compared. Ongoing work is aimed at explicitly investigating the dynamical similarities and differences in these systems. A major focus of this work involves exploiting insight gained from the previous studies of the S3T system. The close connection between the dynamics of the RNL and S3T models and the similarities between the structural features of the rolls and streaks that play a key role in the S3T and RNL dynamics provides evidence that the same mechanisms are operating in these systems. The SSP of the S3T system is well understood and ongoing work aims to characterize the extent to which this same SSP operates in the RNL dynamics. Forming a successful connection between these SSPs and that of the DNS holds the promise of providing insight into the dynamics of wall-turbulence.

APPENDIX: DETAILS OF THE S3T/RNL SYSTEM FORMULATION

The operator $A(\mathbf{U})$ in (3) is obtained by taking the divergence of (2b) and using continuity (1c) and $\nabla \cdot \mathbf{e} = 0$ to express the pressure as

$$p = -\Delta^{-1} \left[\nabla \cdot (\mathbf{U} \cdot \nabla \mathbf{u} + \mathbf{u} \cdot \nabla \mathbf{U}) \right], \tag{A1}$$

so that

$$A(\mathbf{U})\mathbf{u} = -\mathbf{U} \cdot \nabla \mathbf{u} - \mathbf{u} \cdot \nabla \mathbf{U} + \nabla \Delta^{-1} \left[\nabla \cdot (\mathbf{U} \cdot \nabla \mathbf{u} + \mathbf{u} \cdot \nabla \mathbf{U}) \right] + \frac{1}{R} \Delta \mathbf{u}. \tag{A2}$$

In the above, Δ^{-1} is the inverse of the Laplacian, rendered unique by imposition of the no slip boundary conditions at the channel walls.

As described in Sec. II, the S3T system is a second order closure of the NS equations in (1), in which the first order cumulant is $\mathbf{U}$ and the second order nine component cumulant is the spatial covariance at time t of the flow velocities $C \equiv C(1, 2) = \langle \langle \mathbf{u}_1 \otimes \mathbf{u}_2 \rangle \rangle$ between the two points $\mathbf{x}_1 = (x_1, y_1, z_1)$ and $\mathbf{x}_2 = (x_2, y_2, z_2)$ where $\otimes$ is the tensor (outer) product.[68] The ensemble average over forcing realizations is denoted by $\langle \langle \cdot \rangle \rangle$, which under the ergodic assumption is equivalent to the streamwise average, i.e., $\langle \langle \cdot \rangle \rangle \equiv \langle \cdot \rangle$. The flow then evolves according to (4), which is restated here for clarity:

$$\mathbf{U}_t = -\mathbf{U} \cdot \nabla \mathbf{U} - \nabla P + \frac{1}{R} \Delta \mathbf{U} + \mathcal{L}C,$$

$$C_t = (A_1(\mathbf{U}) + A_2(\mathbf{U})) \, C + Q,$$

where $\mathbf{A}_1(\mathbf{U})C = \langle (A_1(\mathbf{U})\mathbf{u}_1) \otimes \mathbf{u}_2 \rangle$ indicates the contribution to the time rate of change of the covariance from the action of the operator $A(\mathbf{U})$, evaluated at point $\mathbf{x}_1$, on the corresponding component of C, and a similar relation holds for $\mathbf{A}_2(\mathbf{U})C$. $Q = \langle \langle \mathbf{e}_1 \otimes \mathbf{e}_2 \rangle \rangle$ is the second order covariance of the stochastic excitation under the assumption that the noise is temporally delta correlated. The mean equation (4a) is forced by the divergence of the perturbation Reynolds stresses $-\langle \mathbf{u} \cdot \nabla \mathbf{u} \rangle$ and this term can be expressed as a linear function of the covariance, $\mathcal{L}C$.

If (4a) is considered to be forced independently by a specified Reynolds stress divergence specified symbolically as $\mathcal{L}C$, then the mean flow dynamics (4a) define a forced streamwise constant or 2D/3C model of the flow field.[35,41] The S3T system is obtained by closing the dynamics through the coupling of the perturbation covariance evolution equation (4b) to the streamwise constant 2D/3C model.

[1] J. Kim, P. Moin, and R. Moser, "Turbulence statistics in fully developed channel flow at low Reynolds number," J. Fluid Mech. **177**, 133–166 (1987).

[2] M. Simens, J. Jimenez, S. Hoyas, and Y. Mizuno, "A high-resolution code for turbulent boundary layers," J. Comput. Phys. **228**, 4218–4231 (2009).

[3] J. C. del Álamo, J. Jiménez, P. Zandonade, and R. D. Moser, "Scaling of the energy spectra of turbulent channels," J. Fluid Mech. **500**, 135–144 (2004).

[4] T. Tsukahara, H. Kawamura, and K. Shingai, "DNS of turbulent Couette flow with emphasis on the large-scale structure in the core region," J. Turbul. **7**, 1–16 (2006).

[5] S. Hoyas and J. Jimenez, "Reynolds number effects on the Reynolds-stress budgets in turbulent channels," Phys. Fluids **20**, 101511 (2008).

[6] B. F. Farrell and P. J. Ioannou, "Generalized stability. Part I: Autonomous operators," J. Atmos. Sci. **53**, 2025–2040 (1996).

[7] B. F. Farrell and P. J. Ioannou, "Generalized stability. Part II: Non-autonomous operators," J. Atmos. Sci. **53**, 2041–2053 (1996).

[8] B. F. Farrell, "Optimal excitation of perturbations in viscous shear flow," Phys. Fluids **31**, 2093–2102 (1988).

[9] K. M. Butler and B. F. Farrell, "Three-dimensional optimal perturbations in viscous shear flows," Phys. Fluids **4**, 1637–1650 (1992).

[10] L. H. Gustavsson, "Energy growth of three-dimensional disturbances in plane Poiseuille flow," J. Fluid Mech. **224**, 241–260 (1991).

[11] L. N. Trefethen, A. E. Trefethen, S. C. Reddy, and T. A. Driscoll, "Hydrodynamic stability without eigenvalues," Science **261**, 578–584 (1993).

[12] S. C. Reddy and D. S. Henningson, "Energy growth in viscous shear flows," J. Fluid Mech. **252**, 209–238 (1993).

[13] B. F. Farrell and P. J. Ioannou, "Stochastic forcing of the linearized Navier-Stokes equations," Phys. Fluids A **5**, 2600–2609 (1993).

[14] B. Bamieh and M. Dahleh, "Energy amplification in channel flows with stochastic excitation," Phys. Fluids **13**, 3258–3269 (2001).

[15] M. R. Jovanović and B. Bamieh, "Componentwise energy amplification in channel flows," J. Fluid Mech. **534**, 145–183 (2005).

[16] D. S. Henningson, "Comment on "Transition in shear flows. Nonlinear normality versus non-normal linearity" [Phys. Fluids **7**, 3060 (1995)]," Phys. Fluids **8**, 2257–2258 (1996).

[17] D. S. Henningson and S. C. Reddy, "On the role of linear mechanisms in transition to turbulence," Phys. Fluids **6**, 1396–1398 (1994).

[18] K. M. Butler and B. F. Farrell, "Optimal perturbations and streak spacing in turbulent shear flow," Phys. Fluids A **5**, 774–777 (1993).

[19] J. Kim and J. Lim, "A linear process in wall bounded turbulent shear flows," Phys. Fluids **12**, 1885–1888 (2000).

[20] F. Waleffe, J. Kim, and J. M. Hamilton, "On the origin of streaks in turbulent shear flows," in *Turbulent Shear Flows*, edited by F. Durst, R. Friedrich, B. Schmidt, B. Launder, F. Schumann, and J. Whitelaw (Springer-Verlag, Munich, Germany, 1993), Vol. 8, pp. 37–49.

[21] M. R. Jovanović and B. Bamieh, "Modeling flow statistics using the linearized Navier-Stokes equations," in *Proceedings of the 40th IEEE Conference on Decision and Control, Orlando, FL* (IEEE, New York, NY, 2001), Vol. 5, pp. 4944–4949.

[22] B. F. Farrell and P. J. Ioannou, "Perturbation structure and spectra in turbulent channel flow," Theor. Comput. Fluid Dyn. **11**, 237–250 (1998).

[23] J. C. del Álamo and J. Jiménez, "Linear energy amplification in turbulent channels," J. Fluid Mech. **559**, 205–213 (2006).

[24] Y. Hwang and C. Cossu, "Amplification of coherent structures in the turbulent Couette flow: an input-output analysis at low Reynolds number," J. Fluid Mech. **643**, 333–348 (2010).

[25] C. Cossu, G. Pujals, and S. Depardon, "Optimal transient growth and very large scale structures in turbulent boundary layers," J. Fluid Mech. **619**, 79–94 (2009).

[26] R. Moarref and M. R. Jovanović, "Model-based design of transverse wall oscillations for turbulent drag reduction," J. Fluid Mech. **707**, 205–240 (2012).

[27] L. Sirovich, "Turbulence and the dynamics of coherent structures. I - Coherent structures. II - Symmetries and transformations. III - Dynamics and scaling," Q. Appl. Math. **45**, 561–571 (1987).

[28] T. R. Smith, J. Moehlis, and P. Holmes, "Low-dimensional modelling of turbulence using the proper orthogonal decomposition: A tutorial," Nonlinear Dyn. **41**, 275–307 (2005).

[29] J. Jiménez, G. Kawahara, M. P. Simens, M. Nagata, and M. Shiba, "Characterization of near-wall turbulence in terms of equilibrium and bursting solutions," Phys. Fluids **17**, 015105 (2005).

[30] G. Kawahara, M. Uhlmann, and L. Van Veen, "The significance of simple invariant solutions in turbulent flows," Annu. Rev. Fluid Mech. **44**, 203–225 (2012).

[31] M. Nagata, "Three-dimensional traveling-wave solutions in plane Couette flow," J. Fluid Mech. **217**, 519–527 (1990).

[32] J. F. Gibson, J. Halcrow, and P. Cvitanović, "Equilibrium and travelling-wave solutions of plane Couette flow," J. Fluid Mech. **638**, 243–266 (2009).

[33] W. C. Reynolds and S. C. Kassinos, "One-point modelling of rapidly deformed homogeneous turbulence," Proc. R. Soc. London, Ser. A **451**, 87–104 (1995).

[34] K. M. Bobba, B. Bamieh, and J. C. Doyle, "Highly optimized transitions to turbulence," in *Proceedings of the 41st IEEE Conference on Decision and Control, Las Vegas, NV* (IEEE, New York, NY, 2002), pp. 4559–4562.

[35] D. F. Gayme, B. J. McKeon, A. Papachristodoulou, B. Bamieh, and J. C. Doyle, "A streamwise constant model of turbulence in plane Couette flow," J. Fluid Mech. **665**, 99–119 (2010).

[36] K. J. Kim and R. J. Adrian, "Very large scale motion in the outer layer," Phys. Fluids **11**, 417–422 (1999).

[37] M. Guala, S. E. Hommema, and R. J. Adrian, "Large-scale and very-large-scale motions in turbulent pipe flow," J. Fluid Mech. **554**, 521–542 (2006).

[38] N. Hutchins and I. Marusic, "Evidence of very long meandering features in the logarithmic region of turbulent boundary layers," J. Fluid Mech. **579**, 1–28 (2007).

[39] B. J. McKeon and A. S. Sharma, "A critical-layer framework for turbulent pipe flow," J. Fluid Mech. **658**, 336–382 (2010).

[40] D. F. Gayme, B. J. McKeon, B. Bamieh, A. Papachristodoulou, and J. C. Doyle, "Amplification and nonlinear mechanisms in plane Couette flow," Phys. Fluids **23**, 065108 (2011).

[41] K. M. Bobba, "Robust flow stability: Theory, computations and experiments in near wall turbulence," Ph.D. thesis (California Institute of Technology, Pasadena, CA, USA, 2004).

[42] A proof of this fact and the explicit construction of a Lyapunov function based on private communications with A. Papachristodoulou and B. Bamieh is provided in Ref. 69.

[43] B. F. Farrell and P. J. Ioannou, "Structural stability of turbulent jets," J. Atmos. Sci. **60**, 2101–2118 (2003).

[44] T. DelSole and B. F. Farrell, "The quasi-linear equilibration of a thermally maintained stochastically excited jet in a quasigeostrophic model," J. Atmos. Sci. **53**, 1781–1797 (1996).

[45] T. DelSole, "Stochastic models of quasigeostrophic turbulence," Surv. Geophys. **25**, 107–194 (2004).

[46] J. B. Marston, E. Conover, and T. Schneider, "Statistics of an unstable barotropic jet from a cumulant expansion," J. Atmos. Sci. **65**, 1955–1966 (2008).

[47] S. M. Tobias, K. Dagon, and J. B. Marston, "Astrophysical fluid dynamics via direct numerical simulation," Astrophys. J. **727**, 127 (2011).

[48] K. Srinivasan and W. R. Young, "Zonostrophic instability," J. Atmos. Sci. **69**, 1633–1656 (2012).

[49] B. F. Farrell, D. F. Gayme, P. Ioannou, B. Lieu, and M. R. Jovanović, "Dynamics of the roll and streak structure in transition and turbulence," in *Proceedings of the Center for Turbulence Research Summer Program* (Center for Turbulence Research, Stanford, CA, 2012), pp. 34–54.

[50] S. J. Kline, W. C. Reynolds, F. A. Schraub, and P. W. Runstadler, "The structure of turbulent boundary layers," J. Fluid Mech. **30**, 741–773 (1967).

[51] M. T. Landahl, "A note on an algebraic instability of inviscid parallel shear flows," J. Fluid Mech. **98**, 243 (1980).

[52] J. D. Swearingen and R. F. Blackwelder, "The growth and breakdown of streamwise vortices in the presence of a wall," J. Fluid Mech. **182**, 255–290 (1987).

[53] H. P. Bakewell Jr. and J. L. Lumley, "Viscous sublayer and adjacent wall region in turbulent pipe flow," Phys. Fluids **10**, 1880–1889 (1967).

[54] F. Waleffe, "Hydrodynamic stability and turbulence: Beyond transients to a self-sustaining process," Stud. Appl. Math. **95**, 319–343 (1995).

[55] J. M. Hamilton, J. Kim, and F. Waleffe, "Regeneration mechanisms of near-wall turbulence structures," J. Fluid Mech. **287**, 317–348 (1995).

[56] F. Waleffe, "On a self-sustaining process in shear flows," Phys. Fluids **9**, 883–900 (1997).

[57] P. Hall and S. Sherwin, "Streamwise vortices in shear flows: Harbingers of transition and the skeleton of coherent structures," J. Fluid Mech. **661**, 178–205 (2010).

[58] W. Schoppa and F. Hussain, "Coherent structure generation in near-wall turbulence," J. Fluid Mech. **453**, 57–108 (2002).

[59] B. F. Farrell and P. J. Ioannou, "Optimal excitation of three dimensional perturbations in viscous constant shear flow," Phys. Fluids **5**, 1390–1400 (1993).

[60] B. F. Farrell and P. J. Ioannou, "Dynamics of streamwise rolls and streaks in turbulent wall-bounded shear flow," J. Fluid Mech. **708**, 149–196 (2012).

[61] J. Jiménez, "Near-wall turbulence," Phys. Fluids **25**, 101302 (2013).

[62] J. F. Gibson, "Channelflow: A spectral Navier-Stokes simulator in C++," Technical Report (University of New Hampshire, 2014), see Channelflow.org.

[63] J. F. Gibson, J. Halcrow, and P. Cvitanović, "Visualizing the geometry of state space in plane Couette flow," J. Fluid Mech. **611**, 107–130 (2008); e-print arXiv:0705.3957.

[64] R. Peyret, *Spectral Methods for Incompressible Flows* (Springer-Verlag, 2002).

[65] C. Canuto, M. Hussaini, A. Quateroni, and T. Zhang, *Spectral Methods in Fluid Dynamics* (Springer-Verlag, 1988).

[66] T. A. Zang and M. Y. Hussaini, "Numerical experiments on subcritical transition mechanism," AIAA Paper 85-0296, 1985.

[67] N. C. Constantinou, A. Loranzo-Durán, M.-A. Nikolaidis, B. F. Farrell, P. J. Ioannou, and J. Jiménez, "Turbulence in the highly restricted dynamics of a closure at second order: comparison with DNS," J. Phys.: Conf. Ser. **506**, 012004 (2014).

[68] U. Frisch, *Turbulence: The Legacy of A. N. Kolmogorov* (Cambridge University Press, 1995).

[69] D. F. Gayme, "A robust control approach to understanding nonlinear mechanisms in shear flow turbulence," Ph.D. thesis (Caltech, Pasadena, CA, USA, 2010).